Transdermal hydrogen sulfide delivery enabled by open metal site metal-organic frameworks

Ruth M. Mandel,[a,‡] Piyusha S. Lotlikar,[a,‡] Tomče Runčevski,[b] Jung-Hoon Lee,[c] Joshua J. Woods,[a,d,†] Tristan A. Pitt,[a] Justin J. Wilson,[a] Phillip J. Milner [a,*]

[a]Department of Chemistry and Chemical Biology, Cornell University, Ithaca, NY 14850, United States

[b]Department of Chemistry, Southern Methodist University, Dallas, TX 75275, United States

[c]Computational Science Research Center, Korea Institute of Science and Technology (KIST), Seoul 02792, Republic of Korea

[d]Robert F. Smith School for Chemical and Biomedical Engineering, Cornell University, Ithaca, NY 14850, United States

ABSTRACT: Hydrogen sulfide (H_2S) is an endogenously produced gasotransmitter involved in many physiological processes that are integral to proper cellular functioning, including chemical signaling, redox balancing, and modification of vital proteins. Due to its profound anti-inflammatory and antioxidant properties, H_2S plays important roles in preventing inflammatory skin disorders and improving wound healing. Transdermal H_2S delivery is a therapeutically viable option for the management of such disorders. However, current small-molecule H_2S donors are not optimally suited for transdermal delivery and typically generate electrophilic byproducts that may lead to undesired toxicity. Here, we demonstrate that H_2S release from metal-organic frameworks (MOFs) bearing coordinatively unsaturated metal centers is a promising alternative for controlled transdermal delivery of gaseous H_2S without the release of unwanted byproducts. In particular, extensive gas sorption measurements and powder X-ray diffraction (PXRD) studies of eleven MOFs support that the Mg-based framework Mg_2(dobdc) (dobdc^{4-} = 2,5-dioxidobenzene-1,4-dicarboxylate) is uniquely well-suited for transdermal H_2S delivery due to its strong yet completely reversible binding of H_2S, high capacity (14.7 mmol/g or 33.3 wt% at 1 bar and 25 °C), and lack of toxicity. In addition, Rietveld refinement of high-quality synchrotron PXRD data from a H_2S-dosed microcrystalline sample of Mg_2(dobdc) supports that the high H_2S capacity of this framework arises due to the presence of three distinct binding sites: at the Mg centers through a Mg···S interaction (primary site), through a short S···S interaction to the polarized H_2S molecules at the primary sites (secondary site), and in the center of the pores (tertiary site). Last, we demonstrate that transdermal delivery of H_2S from this framework is sustained over a 24 h period through porcine skin. Not only is this significantly longer than sodium sulfide (Na_2S), but this represents the first example of controlled transdermal delivery of pure H_2S gas. Overall, H_2S-loaded Mg_2(dobdc) is an easily accessible, solid-state source of H_2S, enabling safe storage and transdermal delivery of this therapeutically relevant gas.

INTRODUCTION

Since the discovery of endogenously produced hydrogen sulfide (H_2S) in living tissues,[1,2] this toxic, flammable gas has been identified as the third gasotransmitter, joining nitric oxide (NO) and carbon monoxide (CO).[3] Within humans, H_2S is important for maintaining normal physiological functions, as it mitigates inflammation, promotes angiogenesis, and attenuates oxidative stress arising from high levels of reactive oxygen species and related cellular injuries.[4,5] Consequently, H_2S has been investigated as a therapeutic agent for various diseases and disorders, such as hypertension, Alzheimer's disease, ischemia-reperfusion injury, atherosclerosis, and diabetes.[6–8] In addition, H_2S has recently been implicated for the treatment of many skin pathologies and cancers.[9] Abnormally low H_2S levels in skin tissues have been linked to inflammatory disorders, such as psoriasis, as well as to chronic wounds and skin ulcers.[6,10] As such, reliable methods for transdermal H_2S delivery offer the potential for treating these and other skin-related disorders.

Transdermal delivery of gaseous H_2S via small-molecule donors such as sodium sulfide (Na_2S) remains the most attractive current method of administration.[11,12] In addition, incorporation of H_2S prodrugs into various gels, mats, or fibrous polymers as wound dressings has been shown to improve the consistency of H_2S release and offer wound protection.[13–20] However, depending on the method of H_2S release, many of these small molecules suffer from limited stability and undesirable side effects that arise from electrophilic byproducts.[21,22] In addition, the rapid H_2S release

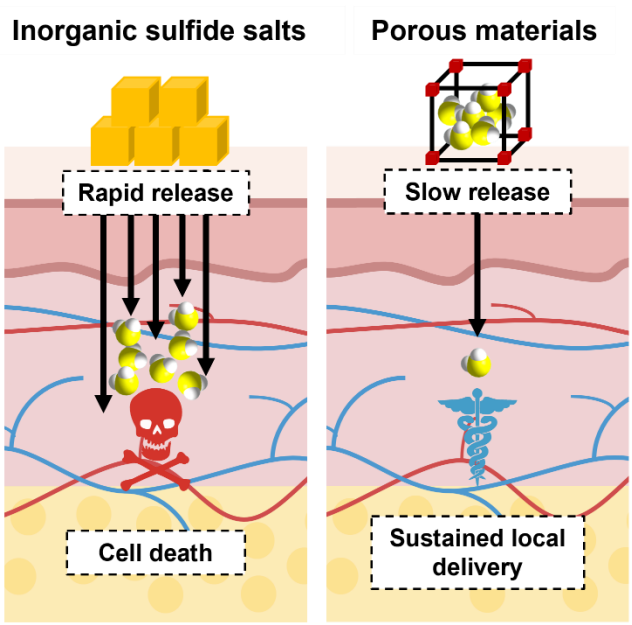

Figure 1. Transdermal H_2S delivery using common inorganic sulfide-containing salts such as Na_2S suffer from rapid H_2S release upon skin contact leading to a high H_2S concentration, resulting in cell death (left). By contrast, slow H_2S release from porous materials such as MOFs may result in improved sustained local H_2S delivery at therapeutic concentrations (right).

from these donors could potentially lead to a high concentration of the gas accumulating at the site of delivery, resulting in local cell death (Fig. 1, left).[19,21] Use of Na_2S in particular often presents difficulties with ensuring consistent dosing due to some volatilization of H_2S post-delivery.[23,24] As an alternative to small-molecule donors, we propose that gaseous H_2S itself can be loaded into porous materials such as metal-organic frameworks (MOFs), providing a promising alternative to traditional H_2S-based therapeutics (Fig. 1, right).[25] The structural tunability of MOFs makes them attractive drug delivery systems (DDS) for active pharmaceutical ingredients, including common drugs, cosmetics, and gasotransmitters.[26–29] Transdermal MOF-based DDS in the form of patches have proved promising for the subcutaneous delivery of drugs such as salicylic acid, ibuprofen, ferulic acid, and caffeine.[30–34] Although MOF-based DDS have been designed for NO[35–37] and CO,[38–40] there have been comparatively few such systems tailored for H_2S delivery.[25,41] Its inherent reactivity and incompatibility with many materials makes constructing a porous material capable of storing and releasing H_2S a major challenge.[42,43]

Recently, we have shown that the biocompatible Zr-based MOF, Zr-fum (fum = fumarate) or MOF-801, is capable of reversibly binding H_2S via hydrogen-bonding interactions between the gas and nodes of the framework.[25] Through triggered release upon exposure to aqueous solution, Zr-fum was able to deliver H_2S to injured cells in an *in vitro* hypoxia-reoxygenation model that simulates ischemia-reperfusion injury. Despite these promising results, Zr-fum rapidly loses H_2S in air, making it unsuitable for transdermal delivery. Gradual, sustained H_2S release is crucial not only to prevent potential cytotoxicity caused by a sudden surge in localized H_2S concentration, but also to mimic endogenous H_2S production rates.[44] We hypothesized that strengthening the interaction between H_2S and the porous framework would lead to slower release under ambient conditions. Because H_2S is Lewis basic, selecting a framework with accessible Lewis acidic sites should result in a much stronger interaction and thus slower H_2S release.[45] For example, MOFs bearing open metal sites or coordinatively unsaturated metal centers represent a diverse class of materials extensively studied for their ability to strongly bind guest molecules through Lewis acid-base interactions.[46] However, their suitability for binding H_2S remains largely unstudied. In addition, there are numerous reports concerning the degradation of MOFs by H_2S, representing an additional challenge.[47]

Herein, we evaluate eleven frameworks from three well-known families of open metal site MOFs for their promise as transdermal H_2S donors. Through gas sorption and cytotoxicity measurements, we demonstrate that only one framework—Mg_2(dobdc) (dobdc^{4-} = 2,5-dioxidobenzene-1,4-dicarboxylate)—exhibits strong, reversible, and high-capacity binding of H_2S coupled with good biocompatibility. Structural characterization via synchrotron powder X-ray diffraction (PXRD) reveals three distinct binding sites of H_2S in the hexagonal channels of the framework, accounting for its very high H_2S capacity (14.7 mmol/g or 33.3 wt% at 1 bar and 25 °C). Using a Franz cell apparatus, we demonstrate that H_2S-loaded Mg_2(dobdc) can sustain H_2S release through porcine skin under ambient conditions over a period of 24 h, significantly longer than a Na_2S control. Taken together, our findings suggest that loading gaseous H_2S into Mg_2(dobdc) represents a promising new avenue for the gradual transdermal delivery of this therapeutically underutilized gas.

RESULTS & DISCUSSION

Although H_2S adsorption has been studied in a range of MOFs,[47–55] the majority of these frameworks are not suitable for therapeutic transdermal delivery. This limitation is a consequence of the presence of toxic or air-sensitive metal centers as well as their relatively weak interaction with H_2S, leading to its rapid loss upon exposure to air.[49] In search of potentially biocompatible materials that may also strongly bind H_2S, we turned to the canonical M_2(dobdc) or MOF-74 family of materials. These frameworks feature rigid one-dimensional hexagonal channels decorated with coordinately unsaturated M^{2+} sites.[56–58] In addition, the Mg variant has previously been used as a drug delivery vehicle.[59] The related isomeric M_2(*m*-dobdc) (*m*-dobdc^{4-} = 2,4-dioxidobenzene-1,3-dicarboxylate) family of frameworks possesses an even higher density of M^{2+} sites capable of interacting strongly with gases such as H_2 and CO_2.[60,61] In addition to the aforementioned materials, the azolate frameworks M_2Cl_2(btdd) (btdd^{2-} = bis(1,2,3-triazolo[4,5-b],[4',5'-*i*]dibenzo[1,4]dioxin)[62] and Ni_3(btp)$_2$ (btp^{3-} = 4,4',4''-(benzene-1,3,5-trityl)tris(pyrazolate))[63] were selected for study due to their potentially enhanced stability toward H_2S.

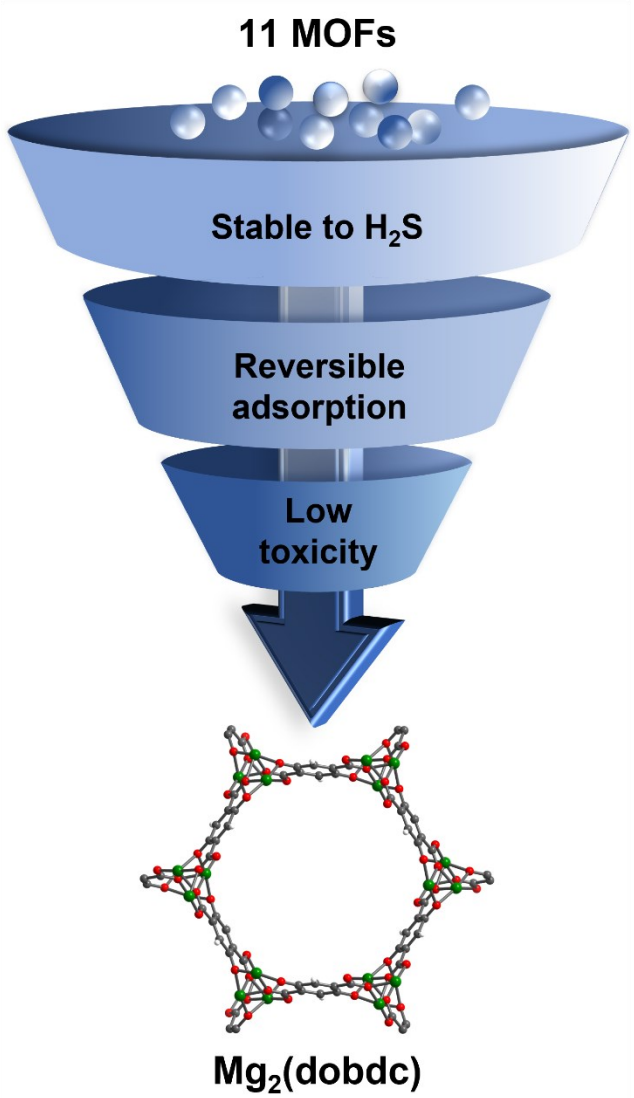

Figure 2. Criteria for the systematic evaluation of eleven open metal site MOFs to determine their suitability for transdermal H_2S delivery, leading to $Mg_2(dobdc)$ as the optimal material.

$M_2Cl_2(btdd)$ MOFs feature an analogous topology to $M_2(dobdc)$ but are more robust due to the higher basicity of their triazolate linkers.[62] Similarly, the high basicity of the pyrazolate linker in $Ni_3(btp)_2$, a framework possessing accessible square planar Ni^{2+} sites, lends it excellent hydrolytic stability.[64]

Based on these criteria, eleven open metal site MOFs were prepared following literature procedures: $M_2(dobdc)$ (M = Mg, Ni, Zn, Cu, Co), $M_2(m\text{-}dobdc)$ (M = Mg, Ni, Co), $M_2Cl_2(btdd)$ (M = Ni, Co), and $Ni_3(btp)_2$ (see supporting information or SI section 2 for details). The successful synthesis and activation of all MOFs were confirmed by PXRD and 77 K N_2 surface area measurements (SI section 2). In order to systematically narrow down these frameworks for H_2S transdermal delivery, they were evaluated based on three key criteria (Fig. 2): (1) the stability of the MOF toward H_2S in solution, (2) the ability of the MOF to reversibly adsorb gaseous H_2S, and (3) the minimal cytotoxicity of the MOF toward human cell lines. First, assessing the stability of frameworks to a solution of H_2S eliminates MOFs that do not retain crystallinity from contention.[64] Pawley refinement of the resulting PXRD pattern allows for further quantification of crystallinity by taking into account the change in the volume weighted average crystalline domain size (LVol-IB) upon H_2S exposure. This additional characterization is crucial to ascertain whether partial dissolution or framework modification may have taken place upon H_2S exposure.[64,65] Second, H_2S adsorption isotherms of frameworks that do retain crystallinity upon exposure to a solution of H_2S allow for the measurement of H_2S sorption properties including reversibility, capacity, and binding strength. Importantly, evaluation of porosity before and after gaseous H_2S exposure ensures fully reversible binding as well as a lack of potential byproducts such as metal sulfides.[66] Last, for these MOFs to be suitable for biomedical applications, they must be nontoxic. *In vitro* cytotoxicity measurements provide a facile means of assessing the potential off-target side effects that may occur when these MOFs are used for transdermal delivery.

In order to quickly eliminate frameworks that are not stable toward H_2S, freshly activated MOFs were submerged in a commercially available solution of H_2S in tetrahydrofuran (THF) under N_2 at 50 °C for 24 h (SI section 3). After this time, any remaining solid was filtered, rinsed with additional THF, and characterized by PXRD to confirm the robustness of the MOF toward H_2S.[64] Upon addition of the H_2S solution, $Cu_2(dobdc)$, $Co_2(dobdc)$, $Co_2(m\text{-}dobdc)$, and $Zn_2(dobdc)$ immediately turned black. After 24 h, no solid could be isolated for these four materials. This observation is consistent with the poor H_2S stability of the Cu and Zn-based MOFs HKUST-1 and MOF-5,[48] respectively, as well as previous findings that $Zn_2(dobdc)$ is not stable toward gaseous H_2S.[25,41] As a strong nucleophile, H_2S likely displaces linkers on the metal nodes, leading to the formation of metal sulfide species. Uniquely among Co-based MOFs, $Co_2Cl_2(btdd)$ appeared to remain crystalline upon visual inspection of the powder pattern after exposure to H_2S solution (SI Fig. S50). The strong metal-nitrogen bonds in this framework likely impart better kinetic stability toward metal sulfide formation.[67] It is important to note, however, that the LVol-IB value calculated from Pawley refinement of the post-H_2S pattern substantially decreased from that of the pristine MOF, suggesting that there may have been some framework dissolution upon H_2S exposure (SI Fig. S51 and S52). Notably, all tested Mg-based ($Mg_2(dobdc)$, $Mg_2(m\text{-}dobdc)$) and Ni-based ($Ni_2(dobdc)$, $Ni_2(m\text{-}dobdc)$, $Ni_2Cl_2(btdd)$, $Ni_3(btp)_2$) frameworks exhibited minimal changes by PXRD upon prolonged exposure to H_2S in solution (SI Fig. S37, S40, S44, S47, S53, and S56).

H_2S adsorption/desorption isotherms were next measured at 25 °C for the seven MOFs that were found to be stable toward H_2S in solution (Fig. 3a, SI section 4). H_2S uptake at 25 °C proved irreversible at low pressures (<50 mbar) for Ni-

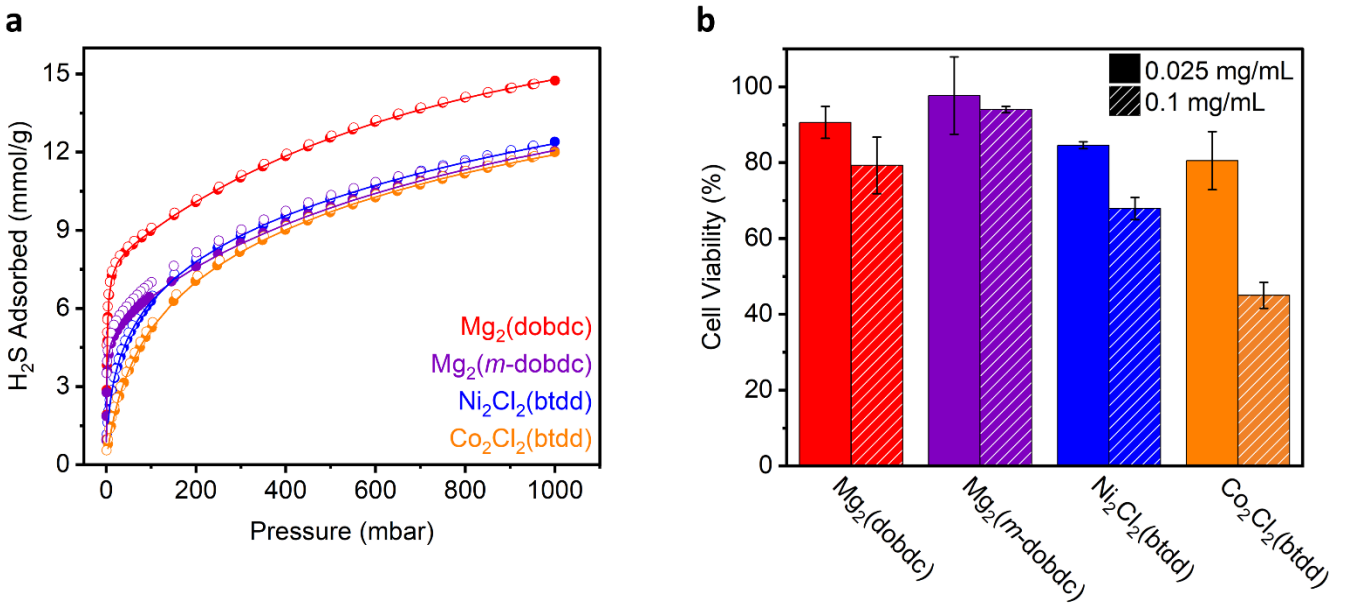

Figure 3. (a) H_2S adsorption (closed circles) and desorption (open circles) isotherms at 25 °C for activated Mg_2(dobdc) (red), Mg_2(*m*-dobdc) (purple), Ni_2Cl_2(btdd) (blue), and Co_2Cl_2(btdd) (orange). Solid lines represent simultaneous fits of the adsorption data to a Langmuir-Freundlich model. A data point was considered equilibrated after <0.01% pressure change occurred over a 45 s interval. (b) Viability of HeLa cells upon exposure to suspensions of Mg_2(dobdc) (red), Mg_2(*m*-dobdc) (purple), Ni_2Cl_2(btdd) (blue), or Co_2Cl_2(btdd) (orange) at concentrations of 0.025 mg/mL (solid) or 0.1 mg/mL (striped) in DMEM supplemented with 10% FBS at 37 °C. Viabilities were determined by incubating the cells with MTT followed by colorimetric analysis using a microplate reader. Results are reported as the average cell viability of 6 wells/concentration compared to untreated cells from three independent trials, with the standard deviation (SD) reported as the error (±SD).

based MOFs Ni_2(dobdc), Ni_2(*m*-dobdc), and Ni_3(btp)$_2$, as indicated by the lack of complete desorption in the H_2S isotherms (SI Fig. S65, S78, and S97, respectively). The Brunauer-Emmett-Teller (BET) surface areas of Ni_2(dobdc) and Ni_2(*m*-dobdc) were found to decrease by 36% and 33%, respectively, after the H_2S sorption isotherms, even with reactivation at 180 °C or 200 °C under high vacuum (10 μbar) (SI Fig. S66 and S79). In addition, X-ray photoelectron spectroscopy (XPS) analysis of Ni_2(dobdc) and Ni_2(*m*-dobdc) after the H_2S isotherms revealed the presence of sulfur-containing species in the high-resolution S2p spectral region, even after extensive evacuation (SI Fig. S72 and S85). It is highly likely from the broad spectral features in this region that multiple sulfur species are present, including polysulfides as well as metal sulfides and sulfates.[68] Rather than just H_2S adsorption on the open Ni^{2+} sites, it is likely that further reactions are taking place inside the pores. Thermogravimetric analysis (TGA) supports this hypothesis, as an expected weight loss attributable to H_2S desorbing from the pores of both frameworks was not observed upon heating up to 600 °C (SI Fig. S70 and S83). Furthermore, both materials exhibited a color change from green to black upon H_2S uptake, indicative of a chemical reaction taking place. The Ni-based MOF Ni_3(btp)$_2$ similarly exhibited a 26% reduction in BET surface area after exposure to gaseous H_2S (SI Fig. S98). Despite this partial loss in porosity due to irreversible H_2S uptake, all three materials retained crystallinity by PXRD, indicating that H_2S exposure does not lead to complete amorphization or to new crystalline phases (SI Fig. S71, S84, and S100). As such, irreversible H_2S uptake (along with Ni allergies being well-established in many people)[69] make these three frameworks unsuitable for transdermal delivery. These findings underline the importance of measuring N_2 uptake before and after H_2S sorption measurements to establish the complete reversibility of H_2S binding in a given material, as retention of crystallinity alone is not enough to establish that a MOF is stable toward H_2S.[41,70]

The four remaining frameworks, Mg_2(dobdc), Mg_2(*m*-dobdc), Co_2Cl_2(btdd), and Ni_2Cl_2(btdd), display fully reversible H_2S adsorption at 25 °C (Fig. 3a). With the exception of Co_2Cl_2(btdd), no evidence of H_2S-mediated decomposition was observed for any of these materials, as all retained full crystallinity (SI Fig. S63, S77, and S96) and porosity (SI Fig. S61, S75, and S94) after H_2S adsorption/desorption measurements. Similar to the results obtained from solution-state H_2S exposure, Co_2Cl_2(btdd) exhibited a substantial loss in crystallite size after gaseous H_2S exposure, indicating some damage to the framework (SI Fig. S90 and S91); however, no corresponding change in surface area was observed (SI Fig. S88).

Though these materials exhibited minimal to no changes in crystallinity and porosity after H_2S exposure, crucial differences in H_2S sorption properties were observed among them. The low-pressure region (<50 mbar) of the isotherms is appreciably steeper for Mg_2(dobdc) and Mg_2(*m*-dobdc) than for Co_2Cl_2(btdd) and Ni_2Cl_2(btdd), indicating that H_2S

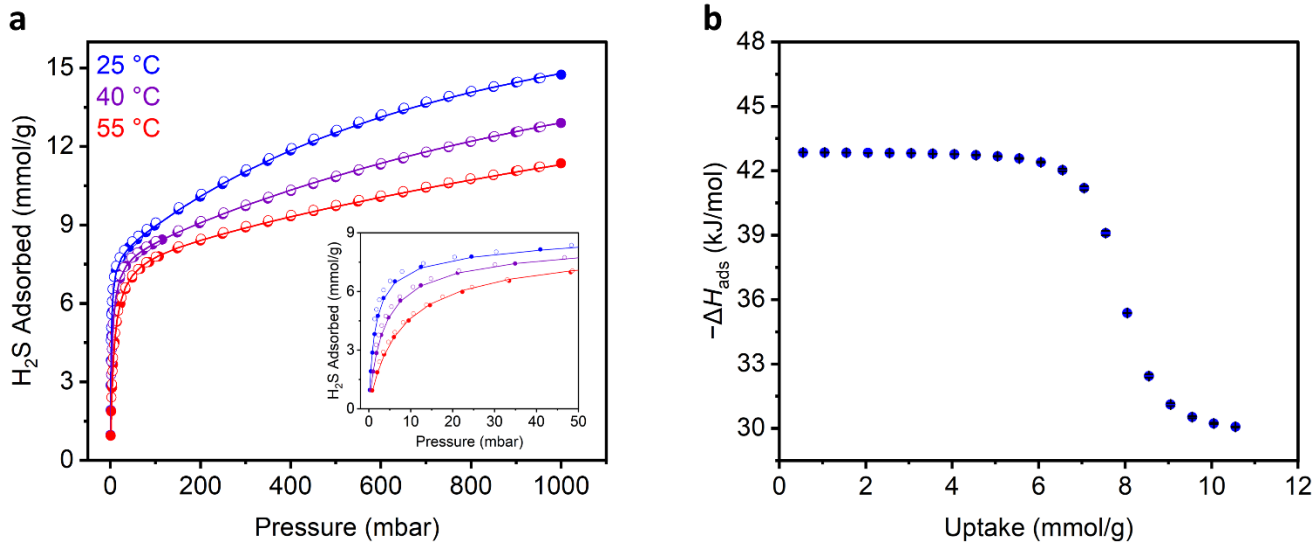

Figure 4. (a) H_2S adsorption (closed circles) and desorption (open circles) isotherms at 25 °C (blue), 40 °C (purple), and 55 °C (red) of activated Mg_2(dobdc). Solid lines represent simultaneous fits of the adsorption data to a Langmuir-Freundlich model. A data point was considered equilibrated after <0.01% pressure change occurred over a 45 s interval. Inset: Low-pressure region up to 50 mbar of the H_2S adsorption isotherms in panel (a). (b) Differential enthalpies of adsorption ($-\Delta H_{ads}$) for H_2S as a function of uptake for activated Mg_2(dobdc) as determined by using the Clausius-Clapeyron equation (eqn. S1) and Langmuir-Freundlich fits in panel (a). Error bars for each data point are too small to see.

binds more strongly in the former two frameworks (see discussion below). This is likely because the stronger field ligands in the azolate-based M_2Cl_2(btdd) MOFs reduce the Lewis acidity of the metal centers. In addition, Mg_2(dobdc) possesses by far the highest H_2S capacity (14.7 mmol/g or 33.3 wt% at 1 bar and 25 °C) among the four MOFs. With such a high potential deliverable capacity, Mg_2(dobdc) concentrations as low as 0.01 mg/mL could deliver H_2S at μM-level therapeutic doses.[71,72] This capacity is among the highest reported to date for a MOF under these conditions, surpassed only by MIL-53(Al)-TDC (18.1 mmol/g).[73] Although Mg_2(*m*-dobdc) should theoretically possess a similar capacity to Mg_2(dobdc), its maximum H_2S uptake at 1 bar is only 12.0 mmol/g. This lower capacity is consistent with its lower BET surface area (1515 m^2/g) compared to Mg_2(dobdc) (1800 m^2/g). Ni_2Cl_2(btdd) and Co_2Cl_2(btdd) exhibit similar capacities to each other under the same conditions (12.4 and 12.0 mmol/g, respectively).

We next evaluated the toxicity of all four materials to determine whether Mg_2(dobdc) is truly the most suitable framework for transdermal H_2S delivery (Fig. 3b, SI section 5). Briefly, HeLa cells were exposed to varying concentrations of the MOFs suspended in Dulbecco's Modified Eagle's Medium (DMEM) supplemented with 10% fetal bovine serum (FBS) for 72 h at 37 °C. To determine viability, cells were then incubated with (4,5-dimethylthiazol-2-yl)-2,5-diphenyltetrazolium bromide (MTT) followed by colorimetric quantification.[74] This was compared to quantification of cells not exposed to the MOF suspension (defined as 100% viability). Mg_2(dobdc) is effectively nontoxic (>90% viability) at concentrations below 0.1 mg/mL, with viabilities dipping to around 80% at this concentration. At all concentrations up to 0.1 mg/mL, Mg_2(*m*-dobdc) also demonstrates excellent compatibility with HeLa cells (Fig. 3b). Both salicylate frameworks are less toxic than Ni_2Cl_2(btdd) and Co_2Cl_2(btdd), further ruling out these two materials as suitable for H_2S delivery. Although the two salicylate frameworks exhibit similarly steep H_2S adsorption properties and minimal toxicities, the higher deliverable capacity of Mg_2(dobdc) makes it the most promising material to evaluate further for transdermal H_2S delivery.

To understand the origin of strong H_2S binding in Mg_2(dobdc), 40 °C and 55 °C H_2S adsorption/desorption isotherms for this material were collected in addition to the 25 °C isotherm (Fig. 4a). For comparison, the same isotherms were collected for Mg_2(*m*-dobdc), Ni_2Cl_2(btdd), and Co_2Cl_2(btdd) as well (SI section 4). The isotherms were fit simultaneously to dual-site Langmuir-Freundlich models to enable calculation of the differential enthalpies of H_2S adsorption ($-\Delta H_{ads}$) as a function of H_2S loading (Fig. 4b). Two distinct binding regimes were observed. At low H_2S loadings, adsorption presumably occurs at the vacant Mg^{2+} sites, with a relatively favorable $-\Delta H_{ads}$ of 42.97 ± 0.01 kJ/mol. Once these primary binding sites are saturated, additional adsorption occurs at weaker secondary binding sites, as evidenced by a sharp dip followed by a plateau at a $-\Delta H_{ads}$ of 30.60 ± 0.04 kJ/mol. The loading at which this transition occurs (~7 mmol/g) is close to the theoretical loading of 8.4 mmol/g assuming one H_2S molecule per Mg^{2+} site. Similar behavior was observed in Mg_2(*m*-dobdc) (SI Fig. S74). Although H_2S adsorption is about 10 kJ/mol stronger at low loadings in this framework (53 kJ/mol vs 43 kJ/mol), the characteristic transition from primary to secondary adsorption sites occurs at lower loadings (4.5 mmol/g) likely due to fewer accessible Mg^{2+} sites, leading to an overall lower H_2S capacity. In contrast, H_2S binding in Co_2Cl_2(btdd) and

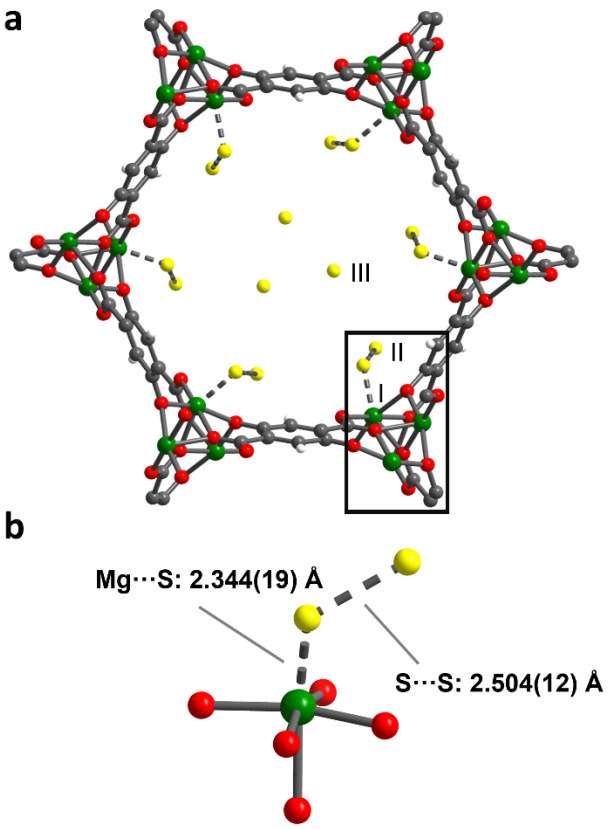

Figure 5. (a) Structural model of Mg_2(dobdc) dosed with 10 mbar of H_2S obtained from Rietveld refinement of synchrotron PXRD data. Primary, secondary, and tertiary adsorption sites are indicated by I, II, and III, respectively. Occupancies for sites I, II, and III, are 0.7676, 0.9201, and 0.9558, respectively. Hydrogen atoms on H_2S molecules were not resolved. (b) Coordination environment of one Mg^{2+} metal site in panel (a) highlighting sites I and II of H_2S adsorption as well as key bond lengths. Gray, white, red, green, and yellow spheres correspond to carbon, hydrogen, oxygen, magnesium, and sulfur, respectively.

Ni_2Cl_2(btdd) becomes significantly less favorable as a function of uptake (SI Fig. S86 and S92), accounting for the shallow adsorption isotherms of these two materials (Fig. 3a).

The preferred H_2S binding mode(s) in Mg_2(dobdc) were probed by synchrotron PXRD collected on H_2S-dosed microcrystalline Mg_2(dobdc) (Fig. 5) and by density functional theory (DFT) calculations (SI section 9). Rietveld refinement of the PXRD pattern of H_2S–Mg_2(dobdc) supports that the primary site of H_2S binding is at the open Mg^{2+} site, with a S···Mg interaction distance of 2.344(19) Å (site I, Fig. 5b). This short distance is consistent with reported magnesium complexes containing thiol or thiolate ligands, which have S···Mg bond distances of 2.3–2.4 Å (SI Table S5).[75–79] The few reported complexes in which either H_2S or SH^- is directly bound to a metal center, including Mn,[80] Os,[81] and Ru[82–85] complexes, also possess comparable metal-sulfur bond distances of 2.33–2.45 Å (SI Table S6). The interaction between H_2S and the Mg^{2+} site in Mg_2(dobdc) is on the shorter side of this range likely due to the small size of the Mg^{2+} cation. Further supporting this short interaction distance, previous structures of water bound in M_2(dobdc) frameworks contain even shorter metal–OH_2 distances (2.1–2.15 Å),[86,87] with an O···Mg interaction in water-bound Mg_2(dobdc) of 2.0892(15) Å.[88] Additional H_2S molecules in the secondary binding site are oriented toward those bound to the primary site through S–S interactions, with a S···S distance of 2.504(12) Å (site II, Fig. 5b). Previous studies on H_2S dimers report a much longer S···S distance of 4.112(1) Å,[89] suggesting that the interaction between H_2S molecules in binding sites I and II in the MOF is more covalent in nature. The strongly polarized Mg–S interaction likely results in a buildup of partial positive charge on the H_2S molecules in binding site I, inducing enhanced interaction with H_2S molecules in binding site II. Consistently, S–S bonds found in polysulfide and disulfide species are even shorter; for example, a typical disulfide bond is around 2.05 Å in length.[90] A DFT-calculated model further supports the presence of the two major H_2S binding sites I and II in Mg_2(dobdc), albeit with slightly longer Mg–S and S–S bond lengths (SI Fig. S128). The calculated binding energies ($-E_b$) of H_2S in sites I (53.5 kJ/mol) and II (32.5 kJ/mol) match well with experimentally obtained $-\Delta H_{ads}$ values (43.0 and 30.6 kJ/mol, respectively). A third binding site in the center of the pore could also be resolved, contributing to the high H_2S capacity of this material (site III, Fig. 5a). Overall, these data support the presence of a strongly polarizing interaction of H_2S with Lewis acidic Mg^{2+} sites, which accounts for a significantly higher H_2S capacity of Mg_2(dobdc) compared to most studied materials developed for transdermal delivery.

Having established that Mg_2(dobdc) strongly and reversibly adsorbs H_2S and is nontoxic to human cells at therapeutic concentrations, we explored whether alternative stimuli to vacuum could trigger H_2S desorption from Mg_2(dobdc) under more biologically relevant conditions. Given the strong binding of water in open metal site MOFs,[91] it is likely that water is capable of facilitating H_2S release from the framework. To test this hypothesis, a known amount of H_2S-dosed Mg_2(dobdc) was suspended in a stirring solution of HEPES buffer (pH 7.4) (SI section 6). From this mixture, aliquots of the suspension were removed at designated time points and analyzed with the fluorescence probe sulfidefluor-7 acetoxymethyl ester (SF7-AM), which exhibits turn-on fluorescence (λ_{max} = 525 nm) upon irreversible reaction with H_2S.[92] The release of H_2S from Mg_2(dobdc) was monitored over time via fluorescence spectroscopy. Upon incubation in this buffer, the concentration of H_2S in solution gradually saturated over a period of 10-20 min and was maintained over 30 min (SI Fig. S109 and S110). Notably, the release rate of H_2S from Mg_2(dobdc) is slower than that from Zr-fum.[25] When H_2S-loaded Zr-fum was suspended in HEPES buffer, peak H_2S concentration in solution was reached rapidly, within only 1 to 2 min, and these levels were maintained for only 10 min (SI Fig. S107 and S108). These results are consistent with the stronger H_2S binding of Mg_2(dobdc) compared to Zr-fum (43 kJ/mol vs. 32 kJ/mol, respectively).[25] This process was concomitant with the conversion of the

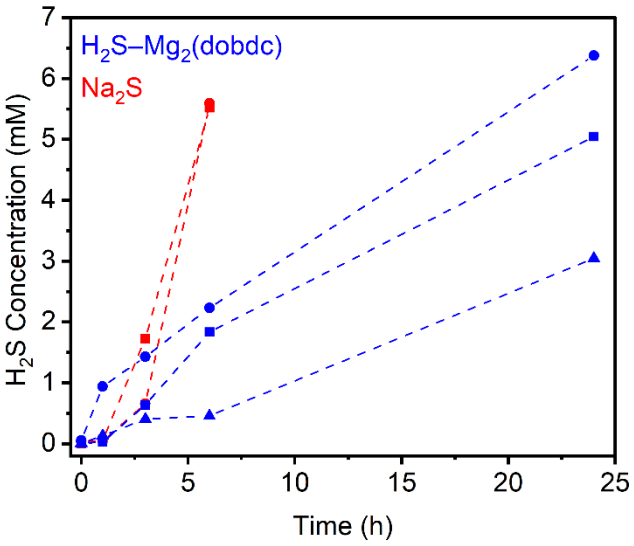

Figure 6. Transdermal H_2S release from $Mg_2(dobdc)$ (blue) and Na_2S (red) through porcine skin detected with SF7-AM via fluorescence spectroscopy over time. Each dotted line with a corresponding shape represents a different trial. H_2S released from $Mg_2(dobdc)$ increases linearly until reaching a maximum at 24 h. By contrast, Na_2S delivers H_2S much more rapidly with the maximum H_2S concentration detected within 6 h.

suspension to a homogeneous solution over the course of 1 h (SI Fig. S113). In addition, UV-Vis spectroscopic monitoring of a suspension of $Mg_2(dobdc)$ in HEPES buffer revealed the gradual formation of an absorbance band at 351 nm, a feature characteristic of free linker presence in solution (SI section 7 and SI Fig. S112). The stability of the $M_2(dobdc)$ family to aqueous conditions has previously been explored,[93,94] and it is known that the $dobdc^{4-}$ linker is prone to protonation resulting in framework dissolution.[64] Nonetheless, depending on the pharmacological mode of administration, such as transdermal delivery, the gradual dissolution of $Mg_2(dobdc)$ in aqueous media could act as a natural means of self-clearance from the body after H_2S delivery, rather than a drawback.

This MOF was next investigated as a transdermal delivery agent for the treatment of skin diseases and disorders (Fig. 6). To this end, an *ex vivo* Franz cell model was used (SI section 8).[11,34] Porcine skin was chosen as a surrogate for human skin due to its similar histological and physiological markers, thickness, and anatomy.[95,96] The porcine dermal samples were collected posthumously and applied as a membrane between the two chambers of the Franz cell. A known amount of H_2S-loaded $Mg_2(dobdc)$ was packed into the top donor chamber while HEPES buffer (pH 7.4) was added to the bottom acceptor chamber (SI Fig. S117). At designated time points, aliquots were removed from the side arm of the acceptor chamber and quenched with SF7-AM solution. A small amount (20 µL) of HEPES buffer was then added to the MOF to facilitate H_2S diffusion from the MOF to skin. The concentration of H_2S in the acceptor chamber was observed to increase slowly over a period of 24 h up to a maximum of between 3 and 6 mM, at which point it began to decrease, likely due to leakage from the Franz cell (Fig. 6, SI Fig. S118, S120, S122). The rate of transdermal H_2S release can be estimated based on the approximate linear increase as 5 µM H_2S/mg MOF/h (SI Fig. S119, S121, S123), well within the therapeutic window with just 5–10 mg of MOF.[97–99] Crucially, a control experiment in which an equivalent amount of Na_2S was packed in the donor chamber instead of the MOF resulted in much more rapid H_2S release, with peak concentrations reached in only 6 h before declining (Fig. 6, SI Fig. S124 and S126). The significantly slower rate of delivery from H_2S-loaded $Mg_2(dobdc)$ is crucial to the successful healing of wounds and other inflammatory skin conditions,[22] indicating that that this material is a much more promising H_2S transdermal delivery agent compared to Na_2S alone.

CONCLUSIONS

Transdermal delivery of H_2S for the treatment of topical wounds and skin diseases and disorders remains a challenge, due to both the hazards of working with gaseous H_2S and the innate difficulty in designing a suitable storage and delivery platform for it. Here, by systematically evaluating the H_2S sorption characteristics and cytotoxicities of eleven open metal site MOFs, we demonstrate that $Mg_2(dobdc)$ is the best for transdermal H_2S delivery. It is clear from these assays that the redox inert Mg^{2+} center in $Mg_2(dobdc)$ facilitates strong H_2S uptake while preventing framework decomposition due to metal sulfide formation. In contrast, H_2S uptake in all tested transition metal-based frameworks is either weak ($M_2Cl_2(btdd)$, M = Co, Ni) or results in (partial) framework destruction (all others). Thus, our findings have important implications for the design of next-generation materials for H_2S capture and delivery.

The outstanding H_2S capacity and binding strength in $Mg_2(dobdc)$ coupled with its nontoxic nature and relative stability in air result in slow transdermal release of H_2S sustained for at least 24 h, significantly longer than an equivalent amount of Na_2S. Future work will focus on integration of the framework into patches or membranes to improve handleability and processability for cutaneous application on animal model systems.

ASSOCIATED CONTENT

Supporting Information.
Synthetic, computational, and crystallographic protocols, as well as all other procedures and data. The Supporting Information is available free of charge at http://pubs.acs.org. The structure of H_2S–$Mg_2(dobdc)$ is available through the Cambridge Crystallographic Data Centre (Deposition #2325508).

AUTHOR INFORMATION

Corresponding Author

* pjm347@cornell.edu

Present Addresses

† Chemical Sciences Division, Lawrence Berkeley National Laboratory, Berkeley, California 94720, United States

Author Contributions

‡ R.M.M. and P.S.L. contributed equally to this work. P.J.M. and J.J. Wilson conceived the project. R.M.M. synthesized and characterized all MOFs and carried out all H_2S adsorption measurements. P.S.L. carried out all transdermal and solution-state H_2S delivery experiments. T.R. refined the structure of H_2S in Mg_2(dobdc). J.-H.L. carried out DFT calculations. J.J. Woods carried out cytotoxicity measurements. T.A.P. conducted Pawley refinements for solution-state H_2S stability assays. The manuscript was written through contributions of all authors. All authors have given approval to the final version of the manuscript.

Funding Sources

This research was supported by the National Institute of General Medical Sciences of the National Institutes of Health under award number R35GM138165 (R.M.M., T.A.P., P.J.M.) and the National Science Foundation under award number CHE-2203369 (P.S.L., J.J. Wilson). The content is solely the responsibility of the authors and does not necessarily represent the official views of the National Institutes of Health or National Science Foundation. We acknowledge the support of a Camille Dreyfus Teacher-Scholar Award to P.J.M. (TC-23-048). Computational works (J.-H.L.) were supported by the KIST Institutional Program (Project No. 2E32531) and the program of Future Hydrogen Original Technology Development (Project No. 2021M3I3A1083946), through the National Research Foundation of Korea (NRF), funded by the Ministry of Science and ICT. Computational resources provided by KISTI Supercomputing Center (Project No. KSC-2021-CRE-0430). Additional support was provided by the American Heart Association Predoctoral Fellowship (J.J. Woods) under award number 20PRE3512039. This work made use of Beamline 11-BM of the Advanced Photon Source. Use of the Advanced Photon Source at Argonne National Laboratory was supported by the U. S. Department of Energy, Office of Science, Office of Basic Energy Sciences, under Contract No. DE-AC02-06CH11357. T.R. acknowledges the support of the Welch Foundation (Grant No. N-2012-20220331).

Notes

The authors declare the following competing financial interest(s): P.J.M. and R.M.M. are listed as co-inventors on several (provisional) patents related to MOFs.

ACKNOWLEDGEMENTS

The authors would like to thank Prof. Joaquin B. Araos (Cornell Department of Veterinary Medicine) for the donation of the porcine skin used for all transdermal experiments and Sijing Meng (Cornell University) for her help in designing figures.

REFERENCES

(1) Abe, K.; Kimura, H. The Possible Role of Hydrogen Sulfide as an Endogenous Neuromodulator. *J. Neurosci.* **1996**, *16* (3), 1066–1071. https://doi.org/10.1523/JNEUROSCI.16-03-01066.1996.

(2) Goodwin, L. R.; Francom, D.; Dieken, F. P.; Taylor, J. D.; Warenycia, M. W.; Reiffenstein, R. J.; Dowling, G. Determination of Sulfide in Brain Tissue by Gas Dialysis/Ion Chromatography: Postmortem Studies and Two Case Reports. *J. Anal. Toxicol.* **1989**, *13* (2), 105–109. https://doi.org/10.1093/jat/13.2.105.

(3) Yang, G.; Sener, A.; Ji, Y.; Pei, Y.; Pluth, M. D. Gasotransmitters in Biology and Medicine: Molecular Mechanisms and Drug Targets. *Oxid. Med. Cell. Longev.* **2016**, *2016*, 1–2. https://doi.org/10.1155/2016/4627308.

(4) Filipovic, M. R.; Zivanovic, J.; Alvarez, B.; Banerjee, R. Chemical Biology of H_2S Signaling through Persulfidation. *Chem. Rev.* **2018**, *118* (3), 1253–1337. https://doi.org/10.1021/acs.chemrev.7b00205.

(5) Vandiver, M. S.; Snyder, S. H. Hydrogen Sulfide: A Gasotransmitter of Clinical Relevance. *J. Mol. Med.* **2012**, *90* (3), 255–263. https://doi.org/10.1007/s00109-012-0873-4.

(6) Xu, M.; Zhang, L.; Song, S.; Pan, L.; Muhammad Arslan, I.; Chen, Y.; Yang, S. Hydrogen Sulfide: Recent Progress and Perspectives for the Treatment of Dermatological Diseases. *J. Adv. Res.* **2021**, *27*, 11–17. https://doi.org/10.1016/j.jare.2020.02.003.

(7) Wallace, J. L.; Wang, R. Hydrogen Sulfide-Based Therapeutics: Exploiting a Unique but Ubiquitous Gasotransmitter. *Nat. Rev. Drug Discov.* **2015**, *14* (5), 329–345. https://doi.org/10.1038/nrd4433.

(8) Song, Z.; Zhao, L.; Ma, T.; Osama, A.; Shen, T.; He, Y.; Fang, J. Progress and Perspective on Hydrogen Sulfide Donors and Their Biomedical Applications. *Med. Res. Rev.* **2022**, *42* (5), 1930–1977. https://doi.org/10.1002/med.21913.

(9) Xiao, Q.; Xiong, L.; Tang, J.; Li, L.; Li, L. Hydrogen Sulfide in Skin Diseases: A Novel Mediator and Therapeutic Target. *Oxid. Med. Cell. Longev.* **2021**, *2021*, 1–11. https://doi.org/10.1155/2021/6652086.

(10) Coavoy-Sánchez, S. A.; Costa, S. K. P.; Muscará, M. N. Hydrogen Sulfide and Dermatological Diseases. *Br. J. Pharmacol.* **2020**, *177* (4), 857–865. https://doi.org/10.1111/bph.14699.

(11) Marwah, M. K.; Shokr, H.; Sanchez-Aranguren, L.; Badhan, R. K. S.; Wang, K.; Ahmad, S. Transdermal Delivery of a Hydrogen Sulphide Donor, ADT-OH Using Aqueous Gel Formulations for the Treatment of Impaired Vascular Function: An Ex Vivo Study. *Pharm. Res.* **2022**, *39* (2), 341–352. https://doi.org/10.1007/s11095-021-03164-z.

(12) Marwah, M. K.; Manhoosh, B.; Shokr, H.; Al Tahan, M. A.; Stewart, R.; Iqbal, M.; Sanchez, L. D.; Abdullah, S.; Ahmad, S.; Wang, K.; Rana, K. S.; Sanchez-Aranguren, L. Transdermal Delivery of Mitochondrial-Targeted Hydrogen Sulphide Donor, AP39 Protects against 6-Hydroxydopamine-Induced Mitochondrial Dysfunction. *Eur. J. Pharm. Biopharm.* **2023**, *191*, 166–174. https://doi.org/10.1016/j.ejpb.2023.09.004.

(13) Lu, C.; Li, Y.; Zhu, W.; Yang, Y.; Liu, K.; Li, Q.; Gao, M. A Theranostic Probe for Promotion of Skin Wound Healing by Exudate-Triggered H_2S Release with Self-Monitoring Ability. *ACS Appl. Bio Mater.* **2023**, *6* (2), 674–680. https://doi.org/10.1021/acsabm.2c00919.

(14) Wu, J.; Chen, A.; Zhou, Y.; Zheng, S.; Yang, Y.; An, Y.; Xu, K.; He, H.; Kang, J.; Luckanagul, J. A.; Xian, M.; Xiao, J.; Wang, Q. Novel H_2S-Releasing Hydrogel for Wound Repair via in Situ Polarization of M2 Macrophages. *Biomaterials* **2019**, *222*, 119398. https://doi.org/10.1016/j.biomaterials.2019.119398.

(15) Wu, J.; Li, Y.; He, C.; Kang, J.; Ye, J.; Xiao, Z.; Zhu, J.; Chen, A.; Feng, S.; Li, X.; Xiao, J.; Xian, M.; Wang, Q. Novel H_2S

Releasing Nanofibrous Coating for In Vivo Dermal Wound Regeneration. *ACS Appl. Mater. Interfaces* **2016**, *8* (41), 27474–27481. https://doi.org/10.1021/acsami.6b06466.

(16) Zhao, X.; Liu, L.; An, T.; Xian, M.; Luckanagul, J. A.; Su, Z.; Lin, Y.; Wang, Q. A Hydrogen Sulfide-Releasing Alginate Dressing for Effective Wound Healing. *Acta Biomater.* **2020**, *104*, 85–94. https://doi.org/10.1016/j.actbio.2019.12.032.

(17) Yuan, F.; He, X.; Lu, Y.; Ning, L.; Zhao, X.; Zhang, S.; Guan, F.; Guo, Y.; Zhang, J. Photoactivated Hydrogen Sulfide Donor with a Near-Infrared Fluorescence Report System for Accelerated Chronic Wound Healing. *Anal. Chem.* **2023**, *95* (17), 6931–6939. https://doi.org/10.1021/acs.analchem.3c00230.

(18) Han, X.; Wang, L.; Shang, Y.; Liu, X.; Yuan, J.; Shen, J. Hydrogen Sulfide-Releasing Polyurethane/Gelatin/Keratin–TA Conjugate Mats for Wound Healing. *J. Mater. Chem. B* **2022**, *10* (42), 8672–8683. https://doi.org/10.1039/D2TB01700H.

(19) Lin, W.-C.; Huang, C.-C.; Lin, S.-J.; Li, M.-J.; Chang, Y.; Lin, Y.-J.; Wan, W.-L.; Shih, P.-C.; Sung, H.-W. In Situ Depot Comprising Phase-Change Materials That Can Sustainably Release a Gasotransmitter H_2S to Treat Diabetic Wounds. *Biomaterials* **2017**, *145*, 1–8. https://doi.org/10.1016/j.biomaterials.2017.08.023.

(20) Lian, J.; Ju, G.; Cai, X.; Cai, Y.; Li, C.; Ma, S.; Cao, Y. Nanofibrous Membrane Dressings Loaded With Sodium Hydrogen Sulfide/Endothelial Progenitor Cells Promote Wound Healing. *Front. Bioeng. Biotechnol.* **2021**, *9*, 657549. https://doi.org/10.3389/fbioe.2021.657549.

(21) Powell, C. R.; Dillon, K. M.; Matson, J. B. A Review of Hydrogen Sulfide (H_2S) Donors: Chemistry and Potential Therapeutic Applications. *Biochem. Pharmacol.* **2018**, *149*, 110–123. https://doi.org/10.1016/j.bcp.2017.11.014.

(22) Shi, X.; Li, H.; Guo, F.; Li, D.; Xu, F. Novel Ray of Hope for Diabetic Wound Healing: Hydrogen Sulfide and Its Releasing Agents. *J. Adv. Res.* **2023**, S2090123223001467. https://doi.org/10.1016/j.jare.2023.05.009.

(23) DeLeon, E. R.; Stoy, G. F.; Olson, K. R. Passive Loss of Hydrogen Sulfide in Biological Experiments. *Anal. Biochem.* **2012**, *421* (1), 203–207. https://doi.org/10.1016/j.ab.2011.10.016.

(24) Kashfi, K.; Olson, K. R. Biology and Therapeutic Potential of Hydrogen Sulfide and Hydrogen Sulfide-Releasing Chimeras. *Biochem. Pharmacol.* **2013**, *85* (5), 689–703. https://doi.org/10.1016/j.bcp.2012.10.019.

(25) Chen, F. E.; Mandel, R. M.; Woods, J. J.; Lee, J.-H.; Kim, J.; Hsu, J. H.; Fuentes-Rivera, J. J.; Wilson, J. J.; Milner, P. J. Biocompatible Metal–Organic Frameworks for the Storage and Therapeutic Delivery of Hydrogen Sulfide. *Chem. Sci.* **2021**, *12* (22), 7848–7857. https://doi.org/10.1039/D1SC00691F.

(26) He, S.; Wu, L.; Li, X.; Sun, H.; Xiong, T.; Liu, J.; Huang, C.; Xu, H.; Sun, H.; Chen, W.; Gref, R.; Zhang, J. Metal-Organic Frameworks for Advanced Drug Delivery. *Acta Pharm. Sin. B* **2021**, *11* (8), 2362–2395. https://doi.org/10.1016/j.apsb.2021.03.019.

(27) Taherzade, S. D.; Rojas, S.; Soleimannejad, J.; Horcajada, P. Combined Cutaneous Therapy Using Biocompatible Metal-Organic Frameworks. *Nanomaterials* **2020**, *10* (12), 2296. https://doi.org/10.3390/nano10122296.

(28) Mallakpour, S.; Nikkhoo, E.; Hussain, C. M. Application of MOF Materials as Drug Delivery Systems for Cancer Therapy and Dermal Treatment. *Coord. Chem. Rev.* **2022**, *451*, 214262. https://doi.org/10.1016/j.ccr.2021.214262.

(29) Maranescu, B.; Visa, A. Applications of Metal-Organic Frameworks as Drug Delivery Systems. *Int. J. Mol. Sci.* **2022**, *23* (8), 4458. https://doi.org/10.3390/ijms23084458.

(30) Márquez, A. G.; Hidalgo, T.; Lana, H.; Cunha, D.; Blanco-Prieto, M. J.; Álvarez-Lorenzo, C.; Boissière, C.; Sánchez, C.; Serre, C.; Horcajada, P. Biocompatible Polymer–Metal–Organic Framework Composite Patches for Cutaneous Administration of Cosmetic Molecules. *J. Mater. Chem. B* **2016**, *4* (43), 7031–7040. https://doi.org/10.1039/C6TB01652A.

(31) Rojas, S.; Colinet, I.; Cunha, D.; Hidalgo, T.; Salles, F.; Serre, C.; Guillou, N.; Horcajada, P. Toward Understanding Drug Incorporation and Delivery from Biocompatible Metal–Organic Frameworks in View of Cutaneous Administration. *ACS Omega* **2018**, *3* (3), 2994–3003. https://doi.org/10.1021/acsomega.8b00185.

(32) Rojas, S.; Wheatley, P. S.; Quartapelle-Procopio, E.; Gil, B.; Marszalek, B.; Morris, R. E.; Barea, E. Metal–Organic Frameworks as Potential Multi-Carriers of Drugs. *CrystEngComm* **2013**, *15* (45), 9364. https://doi.org/10.1039/c3ce41289j.

(33) Rojas, S.; Horcajada, P. Understanding the Incorporation and Release of Salicylic Acid in Metal-Organic Frameworks for Topical Administration. *Eur. J. Inorg. Chem.* **2021**, *2021* (14), 1325–1331. https://doi.org/10.1002/ejic.202001134.

(34) Osorio-Toribio, G.; Velásquez-Hernández, M. D. J.; Mileo, P. G. M.; Zárate, J. A.; Aguila-Rosas, J.; Leyva-Gómez, G.; Sánchez-Sánchez, R.; Magaña, J. J.; Pérez-Díaz, M. A.; Lázaro, I. A.; Forgan, R. S.; Maurin, G.; Lima, E.; Ibarra, I. A. Controlled Transdermal Release of Antioxidant Ferulate by a Porous Sc(III) MOF. *iScience* **2020**, *23* (6), 101156. https://doi.org/10.1016/j.isci.2020.101156.

(35) Yao, S.; Wang, Y.; Chi, J.; Yu, Y.; Zhao, Y.; Luo, Y.; Wang, Y. Porous MOF Microneedle Array Patch with Photothermal Responsive Nitric Oxide Delivery for Wound Healing. *Adv. Sci.* **2022**, *9* (3), 2103449. https://doi.org/10.1002/advs.202103449.

(36) Zhang, P.; Li, Y.; Tang, Y.; Shen, H.; Li, J.; Yi, Z.; Ke, Q.; Xu, H. Copper-Based Metal–Organic Framework as a Controllable Nitric Oxide-Releasing Vehicle for Enhanced Diabetic Wound Healing. *ACS Appl. Mater. Interfaces* **2020**, *12* (16), 18319–18331. https://doi.org/10.1021/acsami.0c01792.

(37) Lin, J.; Ho, W.; Qin, X.; Leung, C.; Au, V. K.; Lee, S. Metal–Organic Frameworks for NO_x Adsorption and Their Applications in Separation, Sensing, Catalysis, and Biology. *Small* **2022**, *18* (13), 2105484. https://doi.org/10.1002/smll.202105484.

(38) Diring, S.; Carné-Sánchez, A.; Zhang, J.; Ikemura, S.; Kim, C.; Inaba, H.; Kitagawa, S.; Furukawa, S. Light Responsive Metal–Organic Frameworks as Controllable CO-Releasing Cell Culture Substrates. *Chem. Sci.* **2017**, *8* (3), 2381–2386. https://doi.org/10.1039/C6SC04824B.

(39) Ma, M.; Noei, H.; Mienert, B.; Niesel, J.; Bill, E.; Muhler, M.; Fischer, R. A.; Wang, Y.; Schatzschneider, U.; Metzler-Nolte, N. Iron Metal–Organic Frameworks MIL-88B and NH_2-MIL-88B for the Loading and Delivery of the Gasotransmitter Carbon Monoxide. *Chem. Eur. J.* **2013**, *19* (21), 6785–6790. https://doi.org/10.1002/chem.201201743.

(40) Silva, A. F.; Calhau, I. B.; Gomes, A. C.; Valente, A. A.; Gonçalves, I. S.; Pillinger, M. Tricarbonyl-Pyrazine-Molybdenum(0) Metal–Organic Frameworks for the Storage and Delivery of Biologically Active Carbon Monoxide. *ACS Biomater. Sci. Eng.* **2023**, *9* (4), 1909–1918. https://doi.org/10.1021/acsbiomaterials.3c00140.

(41) Allan, P. K.; Wheatley, P. S.; Aldous, D.; Mohideen, M. I.; Tang, C.; Hriljac, J. A.; Megson, I. L.; Chapman, K. W.; De Weireld, G.; Vaesen, S.; Morris, R. E. Metal–Organic Frameworks for the Storage and Delivery of Biologically Active Hydrogen Sulfide. *Dalton Trans.* **2012**, *41* (14), 4060. https://doi.org/10.1039/c2dt12069k.

(42) Tonzetich, Z. J. H_2S and Bioinorganic Metal Complexes. In *Hydrogen Sulfide*; Pluth, M. D., Ed.; Wiley, 2022; pp 103–141. https://doi.org/10.1002/9781119799900.ch5.

(43) Woods, J. J.; Wilson, J. J. Bioinorganic Chemistry of Hydrogen Sulfide: Detection, Delivery, and Interactions with Metalloproteins. In *Encyclopedia of Inorganic and Bioinorganic Chemistry*; Scott, R. A., Ed.; Wiley, 2021; pp 1–22. https://doi.org/10.1002/9781119951438.eibc2764.

(44) Olas, B. Hydrogen Sulfide in Signaling Pathways. *Clin. Chim. Acta* **2015**, *439*, 212–218. https://doi.org/10.1016/j.cca.2014.10.037.

(45) Keasler, K. T.; Zick, M. E.; Stacy, E. E.; Kim, J.; Lee, J.-H.; Aeindartehran, L.; Runčevski, T.; Milner, P. J. Handling Fluorinated Gases as Solid Reagents Using Metal-Organic Frameworks. *Science* **2023**, *381* (6665), 1455–1461. https://doi.org/10.1126/science.adg8835.

(46) Kökçam-Demir, Ü.; Goldman, A.; Esrafili, L.; Gharib, M.; Morsali, A.; Weingart, O.; Janiak, C. Coordinatively Unsaturated Metal Sites (Open Metal Sites) in Metal–Organic Frameworks: Design and Applications. *Chem. Soc. Rev.* **2020**, *49* (9), 2751–2798. https://doi.org/10.1039/C9CS00609E.

(47) Martínez-Ahumada, E.; Díaz-Ramírez, M. L.; Velásquez-Hernández, M. D. J.; Jancik, V.; Ibarra, I. A. Capture of Toxic Gases in MOFs: SO_2, H_2S, NH_3 and NO_x. *Chem. Sci.* **2021**, *12* (20), 6772–6799. https://doi.org/10.1039/D1SC01609A.

(48) Liu, J.; Wei, Y.; Li, P.; Zhao, Y.; Zou, R. Selective H_2S/CO_2 Separation by Metal–Organic Frameworks Based on Chemical-Physical Adsorption. *J. Phys. Chem. C* **2017**, *121* (24), 13249–13255. https://doi.org/10.1021/acs.jpcc.7b04465.

(49) Obeso, J. L.; Amaro, D. R.; Flores, C. V.; Gutiérrez-Alejandre, A.; Peralta, R. A.; Leyva, C.; Ibarra, I. A. Chemical Transformations of Highly Toxic H_2S to Promising Clean Energy in MOFs. *Coord. Chem. Rev.* **2023**, *485*, 215135. https://doi.org/10.1016/j.ccr.2023.215135.

(50) Martínez-Ahumada, E.; López-Olvera, A.; Jancik, V.; Sánchez-Bautista, J. E.; González-Zamora, E.; Martis, V.; Williams, D. R.; Ibarra, I. A. MOF Materials for the Capture of Highly Toxic H_2S and SO_2. *Organometallics* **2020**, *39* (7), 883–915. https://doi.org/10.1021/acs.organomet.9b00735.

(51) Li, Y. Research Progress of Hydrogen Sulfide Adsorption Based on MOFs. *ChemistrySelect* **2021**, *6* (37), 9960–9968. https://doi.org/10.1002/slct.202102950.

(52) Georgiadis, A. G.; Charisiou, N.; Yentekakis, I. V.; Goula, M. A. Hydrogen Sulfide (H_2S) Removal via MOFs. *Materials* **2020**, *13* (16), 3640. https://doi.org/10.3390/ma13163640.

(53) Joshi, J. N.; Zhu, G.; Lee, J. J.; Carter, E. A.; Jones, C. W.; Lively, R. P.; Walton, K. S. Probing Metal–Organic Framework Design for Adsorptive Natural Gas Purification. *Langmuir* **2018**, *34* (29), 8443–8450. https://doi.org/10.1021/acs.langmuir.8b00889.

(54) Sánchez-González, E.; Mileo, P. G. M.; Sagastuy-Breña, M.; Álvarez, J. R.; Reynolds, J. E.; Villarreal, A.; Gutiérrez-Alejandre, A.; Ramírez, J.; Balmaseda, J.; González-Zamora, E.; Maurin, G.; Humphrey, S. M.; Ibarra, I. A. Highly Reversible Sorption of H_2S and CO_2 by an Environmentally Friendly Mg-Based MOF. *J. Mater. Chem. A* **2018**, *6* (35), 16900–16909. https://doi.org/10.1039/C8TA05400B.

(55) Hamon, L.; Leclerc, H.; Ghoufi, A.; Oliviero, L.; Travert, A.; Lavalley, J.-C.; Devic, T.; Serre, C.; Férey, G.; De Weireld, G.; Vimont, A.; Maurin, G. Molecular Insight into the Adsorption of H_2S in the Flexible MIL-53(Cr) and Rigid MIL-47(V) MOFs: Infrared Spectroscopy Combined to Molecular Simulations. *J. Phys. Chem. C* **2011**, *115* (5), 2047–2056. https://doi.org/10.1021/jp1092724.

(56) Nguyen-Thuy, T.; Le-Hoang, P.; Hoang Vu, N.; Le, T. N.-M.; Le Hoang Doan, T.; Kuo, J.-L.; Nguyen, T. T.; Phan, T. B.; Nguyen-Manh, D. Hydrogen Adsorption Mechanism of MOF-74 Metal–Organic Frameworks: An Insight from First Principles Calculations. *RSC Adv.* **2020**, *10* (72), 43940–43949. https://doi.org/10.1039/D0RA08864A.

(57) Queen, W. L.; Hudson, M. R.; Bloch, E. D.; Mason, J. A.; Gonzalez, M. I.; Lee, J. S.; Gygi, D.; Howe, J. D.; Lee, K.; Darwish, T. A.; James, M.; Peterson, V. K.; Teat, S. J.; Smit, B.; Neaton, J. B.; Long, J. R.; Brown, C. M. Comprehensive Study of Carbon Dioxide Adsorption in the Metal–Organic Frameworks M_2(Dobdc) (M = Mg, Mn, Fe, Co, Ni, Cu, Zn). *Chem Sci* **2014**, *5* (12), 4569–4581. https://doi.org/10.1039/C4SC02064B.

(58) Rosi, N. L.; Kim, J.; Eddaoudi, M.; Chen, B.; O'Keeffe, M.; Yaghi, O. M. Rod Packings and Metal–Organic Frameworks Constructed from Rod-Shaped Secondary Building Units. *J. Am. Chem. Soc.* **2005**, *127* (5), 1504–1518. https://doi.org/10.1021/ja045123o.

(59) Lawson, S.; Rownaghi, A. A.; Rezaei, F. Combined Ibuprofen and Curcumin Delivery Using Mg-MOF-74 as a Single Nanocarrier. *ACS Appl. Bio Mater.* **2022**, *5* (1), 265–271. https://doi.org/10.1021/acsabm.1c01067.

(60) Kapelewski, M. T.; Geier, S. J.; Hudson, M. R.; Stück, D.; Mason, J. A.; Nelson, J. N.; Xiao, D. J.; Hulvey, Z.; Gilmour, E.; FitzGerald, S. A.; Head-Gordon, M.; Brown, C. M.; Long, J. R. M_2(*m*-Dobdc) (M = Mg, Mn, Fe, Co, Ni) Metal–Organic Frameworks Exhibiting Increased Charge Density and Enhanced H_2 Binding at the Open Metal Sites. *J. Am. Chem. Soc.* **2014**, *136* (34), 12119–12129. https://doi.org/10.1021/ja506230r.

(61) Chen, E. Y.; Mandel, R. M.; Milner, P. J. Evaluating Solvothermal and Mechanochemical Routes towards the

Metal–Organic Framework Mg_2(*m*-Dobdc). *CrystEngComm* **2022**, *24* (41), 7292–7297. https://doi.org/10.1039/D2CE00739H.

(62) Rieth, A. J.; Tulchinsky, Y.; Dincă, M. High and Reversible Ammonia Uptake in Mesoporous Azolate Metal–Organic Frameworks with Open Mn, Co, and Ni Sites. *J. Am. Chem. Soc.* **2016**, *138* (30), 9401–9404. https://doi.org/10.1021/jacs.6b05723.

(63) Colombo, V.; Galli, S.; Choi, H. J.; Han, G. D.; Maspero, A.; Palmisano, G.; Masciocchi, N.; Long, J. R. High Thermal and Chemical Stability in Pyrazolate-Bridged Metal–Organic Frameworks with Exposed Metal Sites. *Chem. Sci.* **2011**, *2* (7), 1311. https://doi.org/10.1039/c1sc00136a.

(64) Wang, Z.; Bilegsaikhan, A.; Jerozal, R. T.; Pitt, T. A.; Milner, P. J. Evaluating the Robustness of Metal–Organic Frameworks for Synthetic Chemistry. *ACS Appl. Mater. Interfaces* **2021**, *13* (15), 17517–17531. https://doi.org/10.1021/acsami.1c01329.

(65) Chen, F. E.; Pitt, T. A.; Okong'o, D. J.; Wetherbee, L. G.; Fuentes-Rivera, J. J.; Milner, P. J. A Structure–Activity Study of Aromatic Acid Modulators for the Synthesis of Zirconium-Based Metal–Organic Frameworks. *Chem. Mater.* **2022**, *34* (7), 3383–3394. https://doi.org/10.1021/acs.chemmater.2c00241.

(66) Hamon, L.; Serre, C.; Devic, T.; Loiseau, T.; Millange, F.; Férey, G.; Weireld, G. D. Comparative Study of Hydrogen Sulfide Adsorption in the MIL-53(Al, Cr, Fe), MIL-47(V), MIL-100(Cr), and MIL-101(Cr) Metal–Organic Frameworks at Room Temperature. *J. Am. Chem. Soc.* **2009**, *131* (25), 8775–8777. https://doi.org/10.1021/ja901587t.

(67) Rieth, A. J.; Wright, A. M.; Dincă, M. Kinetic Stability of Metal–Organic Frameworks for Corrosive and Coordinating Gas Capture. *Nat. Rev. Mater.* **2019**, *4* (11), 708–725. https://doi.org/10.1038/s41578-019-0140-1.

(68) Fantauzzi, M.; Elsener, B.; Atzei, D.; Rigoldi, A.; Rossi, A. Exploiting XPS for the Identification of Sulfides and Polysulfides. *RSC Adv.* **2015**, *5* (93), 75953–75963. https://doi.org/10.1039/C5RA14915K.

(69) Ahlström, M. G.; Thyssen, J. P.; Wennervaldt, M.; Menné, T.; Johansen, J. D. Nickel Allergy and Allergic Contact Dermatitis: A Clinical Review of Immunology, Epidemiology, Exposure, and Treatment. *Contact Dermatitis* **2019**, *81* (4), 227–241. https://doi.org/10.1111/cod.13327.

(70) Chavan, S.; Bonino, F.; Valenzano, L.; Civalleri, B.; Lamberti, C.; Acerbi, N.; Cavka, J. H.; Leistner, M.; Bordiga, S. Fundamental Aspects of H_2S Adsorption on CPO-27-Ni. *J. Phys. Chem. C* **2013**, *117* (30), 15615–15622. https://doi.org/10.1021/jp402440u.

(71) Ying, J.; Wang, Q.; Jiang, M.; Wang, X.; Liu, W.; Wang, X.; Zhang, C.; Xiang, L. Hydrogen Sulfide Promotes Cell Proliferation and Melanin Synthesis in Primary Human Epidermal Melanocytes. *Skin Pharmacol. Physiol.* **2020**, *33* (2), 61–68. https://doi.org/10.1159/000506818.

(72) Yang, C.; Yang, Z.; Zhang, M.; Dong, Q.; Wang, X.; Lan, A.; Zeng, F.; Chen, P.; Wang, C.; Feng, J. Hydrogen Sulfide Protects against Chemical Hypoxia-Induced Cytotoxicity and Inflammation in HaCaT Cells through Inhibition of ROS/NF-κB/COX-2 Pathway. *PLoS ONE* **2011**, *6* (7), e21971. https://doi.org/10.1371/journal.pone.0021971.

(73) Zárate, J. A.; Sánchez-González, E.; Jurado-Vázquez, T.; Gutiérrez-Alejandre, A.; González-Zamora, E.; Castillo, I.; Maurin, G.; Ibarra, I. A. Outstanding Reversible H_2S Capture by an Al(III)-Based MOF. *Chem. Commun.* **2019**, *55* (21), 3049–3052. https://doi.org/10.1039/C8CC09379B.

(74) Mosmann, T. Rapid Colorimetric Assay for Cellular Growth and Survival: Application to Proliferation and Cytotoxicity Assays. *J. Immunol. Methods* **1983**, *65* (1–2), 55–63. https://doi.org/10.1016/0022-1759(83)90303-4.

(75) Burnett, S.; Ferns, R.; Cordes, D. B.; Slawin, A. M. Z.; Van Mourik, T.; Stasch, A. Low-Coordinate Magnesium Sulfide and Selenide Complexes. *Inorg. Chem.* **2023**, *62* (40), 16443–16450. https://doi.org/10.1021/acs.inorgchem.3c02132.

(76) Chadwick, S.; Englich, U.; Senge, M. O.; Noll, B. C.; Ruhlandt-Senge, K. Novel Structural Principles in Magnesium Thiolate Chemistry: Monomers, Trimers, and the First Magnesiate Thiolate. *Organometallics* **1998**, *17* (14), 3077–3086. https://doi.org/10.1021/om980012h.

(77) Ruhlandt-Senge, K. Synthesis and Characterization of the First Three-Coordinate Donor-Free Magnesium Thiolates, $[Mg(STriph)_2]_2$ (Triph = $2,4,6\text{-}Ph_3C_6H_2$) and $[Mg(SMes^*)_2]_2$ (Mes* = $2,4,6\text{-}t\text{-}Bu_3C_6H_2$), and the Four-Coordinate Magnesium Thiolate $Mg(SMes^*)_2(OEt_2)_2$ and Selenolate $Mg(SeMes^*)_2(THF)_2$. *Inorg. Chem.* **1995**, *34* (13), 3499–3504. https://doi.org/10.1021/ic00117a019.

(78) Ren, W.; Gu, D. An Azobenzenyl Anion Radical Complex of Magnesium: Synthesis, Structure, and Reactivity Studies. *Inorg. Chem.* **2016**, *55* (22), 11962–11970. https://doi.org/10.1021/acs.inorgchem.6b02114.

(79) Janssen, M. D.; Van Der Rijst, R.; Spek, A. L.; Grove, D. M.; Van Koten, G. Synthesis and Characterization of Bis(Arenethiolato)Magnesium Complexes with Intramolecular Coordination. X-Ray Structure of $[Mg\{S(C_6H_4\text{-}2\text{-}CH_2NMe_2)\}_2]_2$. *Inorg. Chem.* **1996**, *35* (11), 3436–3439. https://doi.org/10.1021/ic951288+.

(80) Lelj, F. Formation, Crystal Structure and Co-Ordination Chemistry of the [MnIII(Oespz)(SH)] [$Oespz^{2-}$ = 2,3,7,8,12,13,17,18-Octakis(Ethylsulfanyl)-5,10,15,20-Tetraazaporphyrinate Dianion] Complex. *J. Chem. Soc. Dalton Trans.* **1998**, 12, 1985–1992. https://doi.org/10.1039/a708033f.

(81) Esteruelas, M. A.; Fernández, I.; García-Yebra, C.; Martín, J.; Oñate, E. Cycloosmathioborane Compounds: Other Manifestations of the Hückel Aromaticity. *Inorg. Chem.* **2019**, *58* (4), 2265–2269. https://doi.org/10.1021/acs.inorgchem.8b03366.

(82) Sellmann, D.; Lechner, P.; Knoch, F.; Moll, M. Transition-Metal Complexes with Sulfur Ligands. 82. Hydrogen Sulfide, Disulfur, and Carbon Disulfide Molecules as Ligands in Sulfur-Rich $[Ru(PPh_3)('S_4')]$ Complexes [$('S_4')^{2-}$ = 1,2-Bis[(2-Mercaptophenyl)Thio]Ethane$(^{2-})$]. *J. Am. Chem. Soc.* **1992**, *114* (3), 922–930. https://doi.org/10.1021/ja00029a020.

(83) Chandrika, D.; Ma, E. S.; Rettig, S. J.; James, B. R.; Cullen, W. R. Synthesis and X-Ray Structure of an H_2S Complex, $RuCl_2$(P-N)(P(*p*-Tolyl)$_3$)(SH_2) (P-N = *o*-(Diphenylphosphino)-*N*,*N*-Dimethylaniline). *Inorg. Chem.*

1997, *36* (24), 5426–5427. https://doi.org/10.1021/ic9707772.

(84) Ma, E. S. F.; Rettig, S. J.; James, B. R. Extension of the Karplus Relationship to Vicinal Coupling within the P–Ru–S–H Moiety of the H_2S Complexes Cis-RuX_2(P–N)(PPh_3)(SH_2) {X = Cl, Br; P–N = [o-(N,N-Dimethylamino)Phenyl]Diphenylphosphine}. *Chem. Commun.* **1999**, No. 24, 2463–2464. https://doi.org/10.1039/a907360d.

(85) Chatwin, S. L.; Diggle, R. A.; Jazzar, R. F. R.; Macgregor, S. A.; Mahon, M. F.; Whittlesey, M. K. Structure, Reactivity, and Computational Studies of a Novel Ruthenium Hydrogen Sulfide Dihydride Complex. *Inorg. Chem.* **2003**, *42* (24), 7695–7697. https://doi.org/10.1021/ic030241i.

(86) Dietzel, P. D. C.; Morita, Y.; Blom, R.; Fjellvåg, H. An In Situ High-Temperature Single-Crystal Investigation of a Dehydrated Metal–Organic Framework Compound and Field-Induced Magnetization of One-Dimensional Metal–Oxygen Chains. *Angew. Chem. Int. Ed.* **2005**, *44* (39), 6354–6358. https://doi.org/10.1002/anie.200501508.

(87) Dietzel, P. D. C.; Johnsen, R. E.; Blom, R.; Fjellvåg, H. Structural Changes and Coordinatively Unsaturated Metal Atoms on Dehydration of Honeycomb Analogous Microporous Metal–Organic Frameworks. *Chem. - Eur. J.* **2008**, *14* (8), 2389–2397. https://doi.org/10.1002/chem.200701370.

(88) Dietzel, P. D. C.; Blom, R.; Fjellvåg, H. Base-Induced Formation of Two Magnesium Metal-Organic Framework Compounds with a Bifunctional Tetratopic Ligand. *Eur. J. Inorg. Chem.* **2008**, *2008* (23), 3624–3632. https://doi.org/10.1002/ejic.200701284.

(89) Das, A.; Mandal, P. K.; Lovas, F. J.; Medcraft, C.; Walker, N. R.; Arunan, E. The H_2S Dimer Is Hydrogen-Bonded: Direct Confirmation from Microwave Spectroscopy. *Angew. Chem. Int. Ed.* **2018**, *57* (46), 15199–15203. https://doi.org/10.1002/anie.201808162.

(90) Sun, M.; Wang, Y.; Zhang, Q.; Xia, Y.; Ge, W.; Guo, D. Prediction of Reversible Disulfide Based on Features from Local Structural Signatures. *BMC Genomics* **2017**, *18* (1), 279. https://doi.org/10.1186/s12864-017-3668-8.

(91) Li, F.; Hanna, G.; Yücesan, G.; Yazaydin, A. O. Functionalization of Metal–Organic Framework Nanochannels for Water Transport and Purification. *ACS Appl. Nano Mater.* **2023**, *6* (4), 3003–3011. https://doi.org/10.1021/acsanm.2c05389.

(92) Lin, V. S.; Lippert, A. R.; Chang, C. J. Cell-Trappable Fluorescent Probes for Endogenous Hydrogen Sulfide Signaling and Imaging H_2O_2-Dependent H_2S Production. *Proc. Natl. Acad. Sci.* **2013**, *110* (18), 7131–7135. https://doi.org/10.1073/pnas.1302193110.

(93) Zuluaga, S.; Fuentes-Fernandez, E. M. A.; Tan, K.; Xu, F.; Li, J.; Chabal, Y. J.; Thonhauser, T. Understanding and Controlling Water Stability of MOF-74. *J. Mater. Chem. A* **2016**, *4* (14), 5176–5183. https://doi.org/10.1039/C5TA10416E.

(94) Voskanyan, A. A.; Goncharov, V. G.; Novendra, N.; Guo, X.; Navrotsky, A. Thermodynamics Drives the Stability of the MOF-74 Family in Water. *ACS Omega* **2020**, *5* (22), 13158–13163. https://doi.org/10.1021/acsomega.0c01189.

(95) Summerfield, A.; Meurens, F.; Ricklin, M. E. The Immunology of the Porcine Skin and Its Value as a Model for Human Skin. *Mol. Immunol.* **2015**, *66* (1), 14–21. https://doi.org/10.1016/j.molimm.2014.10.023.

(96) Uhm, C.; Jeong, H.; Lee, S. H.; Hwang, J. S.; Lim, K.-M.; Nam, K. T. Comparison of Structural Characteristics and Molecular Markers of Rabbit Skin, Pig Skin, and Reconstructed Human Epidermis for an Ex Vivo Human Skin Model. *Toxicol. Res.* **2023**, *39* (3), 477–484. https://doi.org/10.1007/s43188-023-00185-1.

(97) Lu, H.; Chen, Y.; Hu, P. Current Status and Future Prospects of Hydrogen Sulfide Donor-Based Delivery Systems. *Adv. Ther.* **2023**, *6* (5), 2200349. https://doi.org/10.1002/adtp.202200349.

(98) Iciek, M.; Bilska-Wilkosz, A.; Kozdrowicki, M.; Górny, M. Reactive Sulfur Species in Human Diseases. *Antioxid. Redox Signal.* **2023**, *39* (13–15), 1000–1023. https://doi.org/10.1089/ars.2023.0261.

(99) Han, Y.; Shang, Q.; Yao, J.; Ji, Y. Hydrogen Sulfide: A Gaseous Signaling Molecule Modulates Tissue Homeostasis: Implications in Ophthalmic Diseases. *Cell Death Dis.* **2019**, *10* (4), 293. https://doi.org/10.1038/s41419-019-1525-1.

Insert Table of Contents artwork here